Ethylene polymerization using dealuminated ZSM-2 zeolite nanocrystals as an active metallocene catalyst support

Cristian Covarrubias [a,*], Raúl Quijada [a,b], René Rojas [a,c]

[a] Center for Advanced Interdisciplinary Research in Materials (CIMAT), Universidad de Chile, Avenue Blanco Encalada 2008, Piso Zócalo, Santiago, Chile
[b] Departmento de Ingeniería Química y Biotecnológica, Facultad de Ciencias Físicas y Matemáticas, Universidad de Chile, Santiago, Chile
[c] Departamento de Química Inorgánica, Facultad de Química, Pontificia Universidad Católica de Chile, Santiago, Chile

Keywords:
Ethylene polymerization
Metallocene supports
Metallocene activation
Nanosized zeolites

A B S T R A C T

The preparation of dealuminated (DEAL) ZSM-2 zeolite nanocrystals for use as an active metallocene polymerization catalyst support is presented. The DEAL-ZSM-2 zeolite form was prepared by using steam treatment; metallocene catalyst was directly supported on the zeolite; and evaluated in the polymerization of ethylene using either methylaluminoxane (MAO) or an alkylaluminun as cocatalysts. In order to elucidate the activator effect of the acidic zeolite support, a detailed material characterization was performed.

Metallocene catalyst supported on DEAL-ZSM-2 zeolite exhibited high activity values. The metallocene activation is attributed to the action of soluble cocatalyst (MAO or alkylaluminun) into the reactor and to the activator effect of extraframework aluminum species with strong Lewis acidity existing in the DEAL-ZSM-2 zeolite structure. High external surface area of the nanosized zeolite also contributes to reduce the diffusion effects commonly observed in microsized zeolite supports. The results of this work demonstrate that DEAL-ZSM-2 zeolite support does not necessitate to be treated with MAO previous fixation of the metallocene catalyst, and that polymerization activity can be also achieved using a trialkyaluminum as cocatalyst. Thus, the use of DEAL-ZSM-2 zeolite as metallocene support could contribute to reduce the amount of MAO required for ethylene polymerization.

1. Introduction

The introduction of metallocene-based olefin polymerization catalysts has allowed the production of polyolefins with improved and new properties compared to those obtained through traditional Ziegler-Natta catalysts [1]. The structure and shape of single site metallocene catalysts can profoundly affect the stereochemistry of polymerization, thereby allowing control of the polymer microstructure [2,3]. Some of us have made significant contributions in these research aspects [4–7], as well as in the study of some supported metallocene systems [8–11]. The heterogenization of the soluble metallocene catalysts on preferably inorganic substrates is an essential aspect to make possible the use of these catalytic systems on an industrial scale, proving thus "drop-in" catalysts for use in existing technologies for slurry or gas-phase polymerization processes. Moreover, the use of supported metallocene catalysts reduces reactor fouling with finely dispersed polymer crystals, prevents excessive polymer swelling, and produces polymer particles with a desired regular morphology [12]. Metallocenes by themselves are not active for polymerization, and they require a cocatalyst to generate the active species. Methylaluminoxane (MAO) is known as the most efficient metallocene activator. MAO methylates the dichlorinated metallocene and then, due to its Lewis acidity, it is capable of abstracting one methyl anion to produce the active metallocene monomethyl cation [13]. In the case of supported metallocene catalysts, amorphous and porous silica is the most traditional support material [14,15]. Silica is commonly surface-modified with MAO prior to fixation of the metallocene; the adsorbed MAO allows better fixation of the metallocene on the silica surface and presumably transforms the metallocene into the cationic active species. The activity of this metallocene/MAO/SiO_2 solid system is nevertheless low, and therefore must to be increased by the addition of soluble MAO into the reactor [15]. MAO is a high-cost compound, which has led to the investigation of the use of alternative activators such as trialkylaluminums [16,17], boron-based compounds [18–20], and catalyst supports with active surfaces. According to this last approach, super-acid solid surfaces such as those of sulfated zirconia [21] and sulfated alumina [22] have been shown to produce metallocene activation via metal–carbon bound protonolysis by effect of their Brönsted acidity. Clays treated

* Corresponding author. Tel.: +56 2 978 4855; fax: +56 2 699 3982.
E-mail address: crcovarr@cimat.cl (C. Covarrubias).

with acid and subsequently modified with alkylaluminums have also shown the ability to activate metallocenes [23]. Activation of metallocenes has also been carried out by using borane-functionalized silica using triisobutylaluminum (TIBA) as alkylating agent [24]. In a more recent study, a sulfonic acid functionalized SBA-15 mesoporous silica (SBA-FSO_3H) showed metallocene activation in the presence of trimethylaluminum (TMA) [25]. It has been proposed that the reaction of TMA and the SBA-FSO_3H surface creates a surface-tethered species that can activate the metallocene. From those investigations it can be deduced that surface acid properties of porous solid supports play a determinant role in the activation of the metallocene catalyst. Zeolites are microporous materials known for their surface acid properties, precisely and uniformly sized pore system, suitable chemical and thermal stability, and their proved efficiency as catalysts and catalyst supports in industrially relevant acid catalyzed reactions [26]. In the case of metallocene-catalyzed polymerization of olefins some of the most traditional zeolites have been evaluated as catalyst supports. Michelotti et al. [27] studied the copolymerization of ethylene with higher α-olefins by using metallocenes supported on MAO-treated HY zeolite. They found that the melting points of the copolymers produced were related to a shape selectivity effect promoted by the zeolite support. Ko et al. [28] obtained relatively low ethylene polymerization activities using Cp_2ZrCl_2 metallocene supported on MAO-treated NaY zeolite. Considering the nano-scaled dimensions of the NaY supercage, the authors suggest that active sites inside the supercage of the zeolite should be generated by the coordination of one Cp_2ZrCl_2 molecule with 1–2 MAO molecules. Moreira and Marques [29] used Cp_2ZrCl_2 supported on sodium mordenite zeolite (Na-MOR) for ethylene polymerization. Again only moderate activity values were obtained and it was found that higher amounts of zirconocene fixed on the support led to lower activity values. In later work [30], these authors used H-ZSM-5 zeolite as metallocene support. In this case ethylene polymerization was improved with a MAO pre-contact of the zeolite; this was attributed to the neutralizing effect of MAO on the deactivating Brönsted acid sites of the protonated ZSM-5 zeolite. Acidic H-ZSM-5 zeolite was also evaluated as metallocene support by Damiani and co-workers [31]. The H-ZSM-5 zeolite form was obtained by calcination of NH_4-ZSM-5 zeolite. Polymerization activities using MAO-treated H-ZSM-5 zeolite obtained at 900 °C were significantly higher that those reported in other works. These studies also show that diffusion effects seem to be a limiting factor of the performance of zeolite-supported polymerization catalysts. Until now, to the best of our knowledge, only traditional microsized zeolites have been evaluated as metallocene catalyst supports, and the use of zeolites with nanometer crystal size could reduce the unfavourable diffusion effects as a consequence of a larger external surface area available for the reaction. The preparation of nanosized zeolites has allowed expanding the use of zeolitic materials in emerging application areas, and it is expected to produce significant benefits in the performance of traditional catalytic applications [32]. ZSM-2 zeolite [33,34] is a type of nanosized zeolite that can be obtained with a mean crystal size ranging from about 40 to 200 nm [35], and it has been described as an intergrowth of cubic FAU and hexagonal EMT zeolite-type structures [36,37]. ZSM-2 zeolite consists of 12-membered ring pore openings of ~0.74 nm in diameter. In addition to these structural characteristics and to its high surface area, ZSM-2 zeolite could be prepared with adequate surface acid properties in order to be evaluated as an active support material for metallocene catalysts.

In this work we present the preparation of nanosized ZSM-2 zeolite for its use as an active metallocene polymerization catalyst support. A dealuminated (DEAL) ZSM-2 zeolite form was prepared by using a steam treatment; the metallocene catalyst was directly supported on the zeolite and evaluated in the polymerization of ethylene using MAO as cocatalyst. The polymerization activity of DEAL-ZSM-2 zeolite-supported catalyst was also tested in the presence of an alkylaluminum as cocatalyst. In order to elucidate the activator effect of the acidic zeolite support, a detailed material characterization was performed. For comparative purposes, catalysts supported on traditional amorphous silica were also evaluated.

2. Experimental

2.1. Synthesis of nanosized ZSM-2 zeolite

The molar composition of the synthesized ZSM-2 zeolite nanocrystals was the following: $0.53Li_2O{:}0.5Al_2O_3{:}6TMAOH{:}3.4SiO_2{:}315H_2O$, chosen from a previous report [38]. The synthesis mixture was prepared as follows: a clear lithium–TMA–silicate solution was prepared by mixing adequate amounts of tetraethylorthosilicate (TEOS 98%, Aldrich), lithium hydroxide (LiOH, Stremchemicals > 98%), tetramethylammonium hydroxide (TMAOH, 25% solution in water, Aldrich), and distilled water. Then a TMA–aluminate solution was prepared by dissolving aluminum foil (Al 99.8%, 0.05 mm thick, Aldrich) in TMAOH solution. The latter was slowly added to the lithium–TMA–silicate solution. The clear resultant mixture was added to teflon-lined stainless steel autoclaves and hydrothermally treated at 100 °C. After 24 h of hydrothermal synthesis, the colloidal zeolite product was separated and washed by repeated centrifugation and redispersion in fresh water (7 cycles). The zeolite product was then dried at 110 °C for 2 h and calcined at 550 °C for 6 h, at a heating rate of 10 °C/min.

2.2. Preparation of the dealuminated ZSM-2 zeolite

In order to prepare a more acidic ZSM-2 zeolite form, nanosized ZSM-2 zeolite was submitted to ion exchange by placing 1 g of ZSM-2 zeolite in contact with 100 ml of NH_4NO_3 solution (1 mol/l) at 30 °C for 24 h. Then the NH_4-exchanged sample was thermally treated at 350 °C for 4 h to obtain ZSM-2 zeolite in its protonated form. Protonated ZSM-2 zeolite was subsequently submitted to a dealumination process by using steam treatment. Steaming was performed by placing 1.5 g of the protonated zeolite in a boat-like quartz reactor in a horizontal oven (Thermco, Pacesetter II). Then a water-loaded nitrogen stream (200 cm^3/min) was allowed to enter the oven, and the zeolite sample was steam-treated for 3 h at 600 °C. The water vapour pressure in the nitrogen stream was adjusted to 84.5 kPa. After the steam treatment was completed, the dealuminated zeolite sample (DEAL-ZSM-2) was cooled down to room temperature in a dry nitrogen stream.

2.3. Preparation of supported catalysts

All the operations described here were carried out in a nitrogen atmosphere using Schlenk's technique. Nitrogen was deoxygenated and dried by passing through columns of Cu catalyst and activated molecular sieve (13×), respectively. Toluene was purified by refluxing and freshly distilled under nitrogen from a Na/benzophenone system.

Metallocene bis(*n*-butylcyclopentadienyl) zirconium dichloride ($(nBuCp)_2ZrCl_2$) (Boulder) was directly supported on the prepared zeolites (ZSM-2 and DEAL-ZSM-2) and on MAO-treated ZSM-2 zeolite. Prior to metallocene fixation, the zeolite was dehydrated at 150 °C for 5 h under ultra-high vacuum conditions. (10^{-6} Torr). Metallocene impregnation was carried out by contacting 1 g of dehydrated zeolite with 20 cm^3 of 0.5% $n(BuCp)_2ZrCl_2$ toluene

solution for 30 min at room temperature. The slurry was then filtered through a fritted disk. The resulting solids were washed 3 times with 20 cm^3 of toluene and dried under vacuum for 4 h. For MAO pre-treatment of the zeolite, 1 g of dehydrated zeolite was contacted at 60 °C for 3 h with 20 cm^3 of a 0.56 wt% MAO solution in toluene, which was prepared from a 10% MAO solution (Witco). The resultant solid was washed 3 times with 20 cm^3 of toluene and dried under vacuum for 4 h. For comparison, supported metallocene catalyst was prepared on commercial amorphous silica (EP17G, Crosfield Catalysts) using the same impregnation procedure.

The contents of Zr and Al in supported catalysts were measured by inductively coupled plasma-atomic emission spectroscopy (ICP-AES).

2.4. Ethylene polymerization

Ethylene polymerization was carried out in a 450 ml stainless-steel reactor (Parr), equipped with mechanical stirring and inlets for catalyst suspension, nitrogen and the monomer. For each experiment 3×10^{-6} mol of supported metallocene catalyst were added to the reactor, using an amount of soluble MAO in an Al/Zr = 1500 molar ratio. The polymerization was carried out at 60 °C for 30 min under an ethylene pressure of 2 bars. After this period the polymerization was stopped by quenching with acidified (HCl) ethanol. The polyethylene product was recovered by filtration, washed with ethanol, dried at 40 °C overnight, and then weighed to determine the catalytic activity. Polymerization was also carried out using the unsupported metallocene catalyst under identical reaction conditions.

2.5. Material characterization

ZSM-2 zeolite and the polyethylene products were analyzed by X-ray diffraction (XRD). Powder X-ray diffraction patterns were measured on a Siemens D 5000 diffractometer using Cu Kα radiation within a 2θ range of 5–50° at a scanning speed of 1.2° min^{-1}.

ZSM-2 zeolite nanoparticles and the supported catalysts were examined by high resolution transmission electron microscopy (HRTEM) on a FEI-Tecnai G2 F20 S-Twin HRTEM microscope equipped with a Field Emission Gun (FEG) operating at 120 kV accelerating voltage. Specimens were prepared by transferring a small drop of zeolite–ethanol suspension to carbon-film-coated copper grids. The selected-area electron diffraction (SAED) pattern and channel spacing profile were also obtained for ZSM-2 zeolite. Elemental analysis was also done using energy dispersed X-ray spectrometry (EDX) attached to the microscope.

Scanning electron microscope (SEM) images of polyethylene products were obtained in a Tesla BS 343 SEM microscope. Gold coated specimens were prepared using a sample of fine particle size polymer product.

Diffuse reflectance infrared Fourier-transform (DRIFT) analysis of the zeolite and supported catalysts was carried out in a Bruker Vector 22 FTIR spectrometer using a Harrick diffuse reflectance high-temperature/vacuum chamber (HVC-DRP) with CaF_2 windows. The samples were transferred to the DRIFT chamber into the glob box, and then were in situ heated for 1 h at 150 °C in a constant helium flow. The DRIFT spectra were collected at room temperature, coadding 600 scans at a resolution of 2 cm^{-1}.

The types of acid sites on the support surfaces (ZSM-2 zeolite and reference silica) were identified by FTIR analysis of pyridine sorption. In order to avoid the deactivation of the MAO (highly air sensitive) fixed on an MAO-treated silica support, IR analysis of pyridine sorption was done in an inert atmosphere using a modified procedure through DRIFT system. In this procedure pyridine was directly adsorbed on the powdered samples at 70 °C for 30 min. The pyridine-sorbed sample was then transferred to the DRIFT chamber into a glove box. Physisorbed pyridine was removed from the support surface by flowing helium over the surface for 1 h while keeping the DRIFT chamber at 110 °C. The DRIFT spectra were then collected in a helium flow at 27 °C, coadding 1000 scans at a resolution of 2 cm^{-1}.

Total acidity of zeolite samples was measured using a potentiometric method of titration with *n*-butylamine [39]. *n*-Butylamime (0.1N, 0.05 mL) was added to a dispersion of 0.15 g of zeolite sample in 90 mL of acetonitrile. This system was kept under steady stirring for 3 h. The suspension was then titrated using base solution volumes of 0.05 mL each time. The time elapsed before making a potential measurement was 2 min. The electrode potential variation (mV) was measured with a Hanna PH211 digital pH/mV meter. The maximum acid strength of the first titrated acid surface sites was taken to be the initial electrode potential. The total number of acid sites was estimated from the total amount of base added to reach the plateau in the potential versus volume curve, and the acid site density was calculated considering the apparent surface area value of the corresponding zeolite sample.

Textural characterization of the ZSM-2 zeolite and silica support was done by N_2 adsorption at 77 K in a Micromeritics ASAP 2010 sorptometer. The specific apparent surfaces (S_g) were calculated using the BET equation, and the micropore volume (V_o) by the Dubinin–Radushkevich equation, applied to the experimental data obtained from N_2 adsorption isotherms.

Molar mass distributions of polyethylene products were obtained with a Waters (Alliance GPC 2000) GPC instrument equipped with three Styragel HT-type columns (HT3, HT5, and HT6E). 1,2,4-Trichlorobenzene was used as solvent, at a flow rate of 1 cm^3/min and a temperature of 135 °C. The columns were calibrated with polystyrene standards.

Polymer melting points (T_m) and crystallinities (X_c) were determined by differential scanning calorimetry (DSC), using DSC 2920, TA instruments, equipment calibrated with indium. Heating scans at 10 °C/min from −10 to 170 °C were performed twice.

3. Results and discussion

3.1. Synthesis of nanosized ZSM-2 zeolite

The XRD pattern of the as synthesized ZSM-2 zeolite and that of its dealuminated zeolite form (DEAL-ZSM-2) are shown in Fig. 1. The XRD patterns indicate the presence of a well crystallized ZSM-2 type zeolite phase, with no peaks other than those corresponding to a ZSM-2 zeolite seen [34] (Fig. 1a). It is seen that the crystallinity of ZSM-2 zeolite decreases after submitting it to dealumination by steaming, as judged by the decreased intensity of the most characteristics ZSM-2 XRD peaks (Fig. 1b). The lower crystallinity shown by the DEAL-ZSM-2 form can be explained by the structural changes that occur during partial dealumination of the zeolite framework. The dealumination process involves the elimination of Al from the zeolite framework, and the subsequent healing of the Al vacancies by migration of silicon species as formed from decomposed parts of the framework [40,41]. The dealumination process of ZSM-2 zeolite is schematized in Fig. 2. It is known that the thermal treatment of the NH_4-exchanged zeolite form causes the formation of bridged hydroxyl Si(OH)Al acid groups which exhibit strong Brönsted acidity. Under steaming conditions some of the Al–O bonds of the bridged hydroxyl groups are cleaved and extraframework aluminic (EFAL) species with Lewis acid character

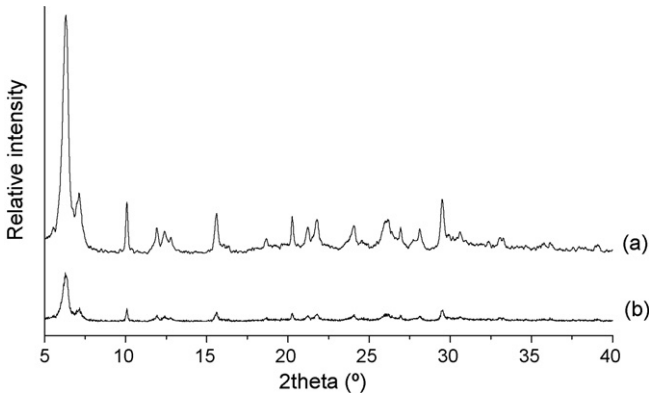

Fig. 1. XRD patterns of (a) ZSM-2 zeolite and (b) DEAL-ZSM-2 zeolite form.

are generated [42]. Species such as AlO^+ and $Al(OH)_2^+$ appear as the main EFAL species identified in steam-dealuminated zeolites [43,44].

ZSM-2 zeolite was also examined by TEM microscopy (Fig. 3). ZSM-2 zeolite can be seen as hexagonal plate-like crystals of ~100 nm in size (Fig. 3a). This crystal morphology is characteristic of the cubic and hexagonal FAU/EMT intergrowth zeolite system [45]. By high-resolution TEM image of the ZSM-2 zeolite (Fig. 3b) it is possible to see a uniform array of channels in some parts of the zeolite crystal which correspond to the ordered zeolite pore system. Channel spacing distribution obtained by HRTEM analysis (Fig. 3c) revealed that the distance between two nonadjacent peaks is equal at 0.774 nm, which is in complete agreement with the crystallographic value known for a 12-ring zeolite pore aperture along the (1 1 1) direction [37]. Diffraction circles of the selected-area electron diffraction pattern confirm the long-range crystalline ordering of the ZSM-2 structure.

The acid and textural properties of the ZSM-2 zeolites are shown in Table 1. Total surface acidity of the zeolite was evaluated by means of the potentiometric method of tritation with *n*-butylamine. The first potential measurement (E_o) indicates that both ZSM-2 zeolite and the DEAL-ZSM-2 zeolite form present very strong surface acidity. DEAL-ZSM-2 zeolite exhibits a higher number and density of acid sites than the initial ZSM-2 zeolite, which can be explained by the creation of Brönsted and Lewis acid sites during deammoniation and dealumination of the zeolite structure. It can be seen that these processes also affect the zeolite textural properties. The large surface area of the nanosized ZSM-2 zeolite is decreased after being transformed into its dealuminated form, which is directly related to the decrease in the micropore volume values produced by the slight partial amorphization and dealumination of the zeolite framework. This decrease in micropore volume of the zeolite is paralleled by an increase in its mesopore volume. The healing of aluminum vacancies during the dealumination involves the migration the silicon species from the zeolite lattice which leaves mesopores behind, i.e. holes formed from resolved weak outer parts of the framework which cannot be repaired by the same mechanism. This dealumination-induced mesoporosity of the DEAL-ZSM-2 zeolite could be a useful property, considering the use of this zeolite as support for bulky metallocene catalyst compounds and during a diffusion-controlled polymerization reaction.

3.2. Preparation of ZSM-2 zeolite-supported metallocene catalysts

The metallocene polymerization catalyst was supported on MAO-treated ZSM-2 zeolite and directly on the ZSM-2 and DEAL-ZSM-2 zeolite forms. Fig. 4a shows an HRTEM image of the metallocene catalyst supported directly on ZSM-2 zeolite. In contrast with the HRTEM image of the pure ZSM-2 zeolite (Fig. 3b), it can be seen that the particles of zircocene occupy the interior of the zeolite channels, as well as some zones of the external surface of the zeolite crystal. From EDX elemental analysis on selected points of the supported catalyst (Fig. 4b) it was found that atomic zirconium concentrations range from 0.02 to 1.03%, which suggests an inhomogeneous distribution of the metallocene in the zeolite crystal. On the other hand, DRIFT spectra of the ZSM-2 zeolite support obtained in the OH-stretching region (Fig. 5) shows a band around 3700 cm^{-1}, which is characteristic of terminal silanol groups (SiOH) existing on the zeolite crystal surface. The OH stretching mode of bridged hydroxyl groups can be seen by the presence of a less intense band around 3667 cm^{-1}. From the intensity of these silanol bands, the population of silanol groups decreases when the metallocene catalyst is supported on ZSM-2 zeolite (Fig. 5b). This indicates that the metallocene reacts with the silanol groups during its fixation on the zeolite surface, and metallocene would be immobilized through the ≡Si–O–ZrCl(nButCp)$_2$ form. This type of silanol–metallocene interaction has already been established for the supporting of

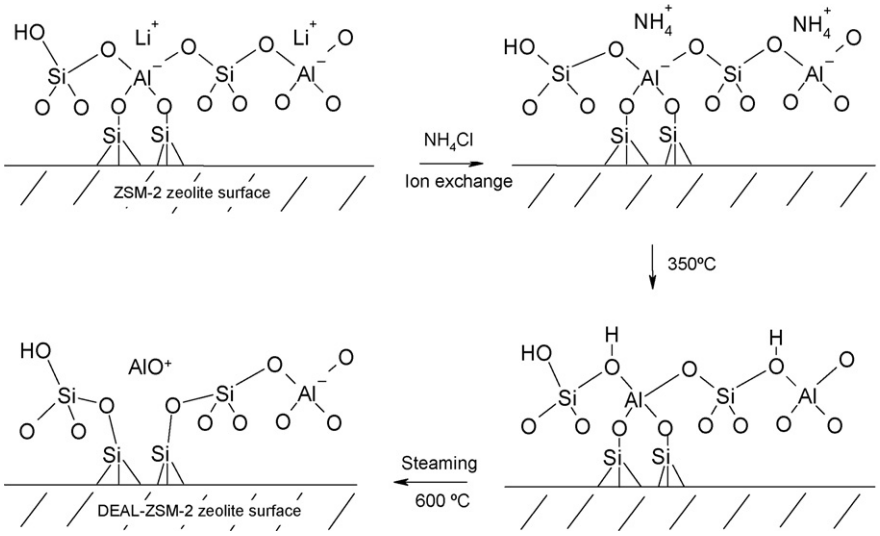

Fig. 2. Dealumination process of ZSM-2 zeolite.

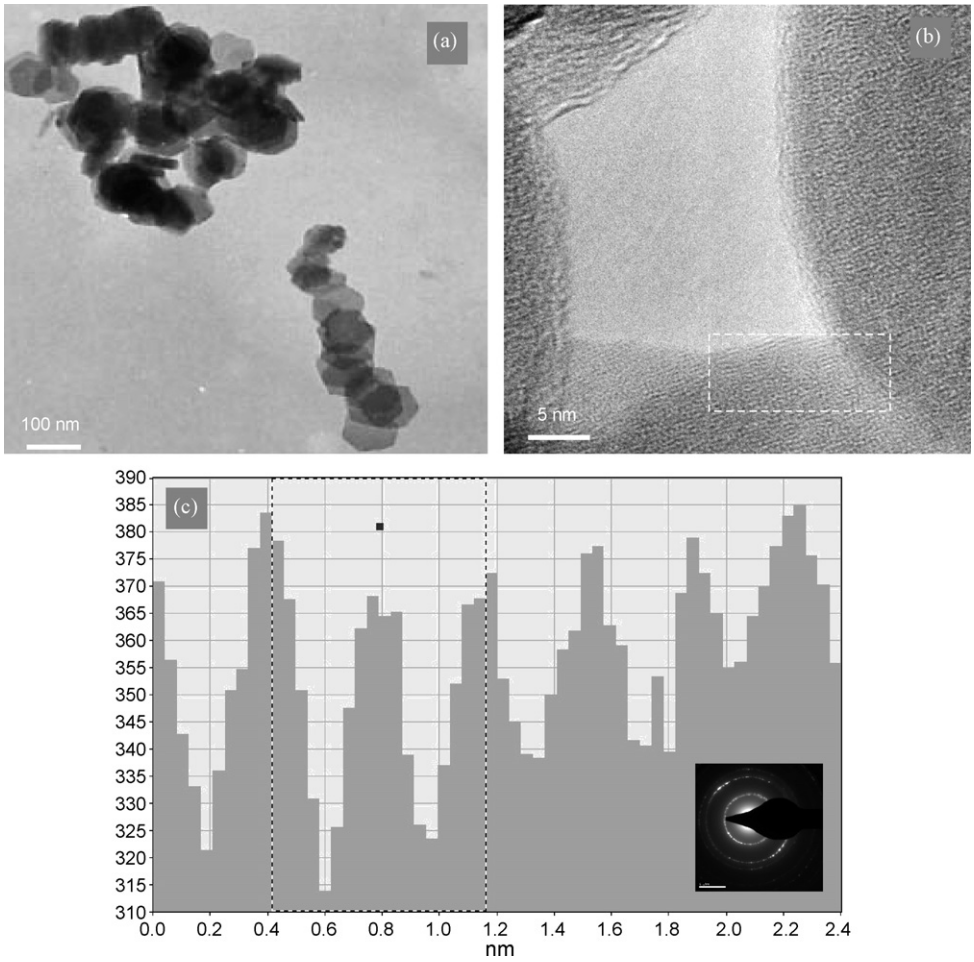

Fig. 3. TEM image of nanosized ZSM-2 zeolite (a), HRTEM image of ZSM-2 zeolite crystals (b), channel spacing distribution of ZSM-2 zeolite structure (c) (inset selected-area electron diffraction pattern SAED).

metallocene on partially dehydroxylated silica surfaces [12]. The bands at 2955 and 2926 cm^{-1}, respectively, correspond to asymmetric CH_3 and CH_2 vibrations, while those at 2894 and 2879 cm^{-1}, respectively, to symmetric CH_3 and CH_2 vibrations from butyl ligands of the metallocene. In the case of the Cat/MAO/ZSM-2 catalyst, the decrease in the DRIFT silanol bands is more pronounced (Fig. 5c) due to reaction of the silanol groups with the highly reactive MAO molecule. In the Cat/MAO/ZSM-2 DRIFT spectrum the bands of the butyl groups of the metallocene are not clearly distinguished due to the predominance of a band centered at 2444 cm^{-1} corresponding to the CH_3 groups of the fixed MAO.

Table 1
Acid and textural properties of ZSM-2 zeolite forms

	ZSM-2	DEAL-ZSM-2
Acidity		
E_o (Mv)	200	242
Total acid strength	(vs)	(vs)
Total number of acid sites (meq g^{-1})	1.70	1.76
Density of acid sites (μeq m^{-2})	2.89	3.54
Textural properties		
Specific surface area (m^2 g^{-1})	588	497
Total pore volume (cm^2 g^{-1})	0.66	0.72
Microporous volume (cm^3 g^{-1})	0.26	0.22
Mesoporous volume (cm^3 g^{-1})	0.40	0.50

$E_o > 100$ mV (vs: very strong site), 0 mV $< E_o <$ 100 mV (s: strong site), −100 mV $< E_o <$ 0 mV (w: weak site), $E_o <$ −100 mV (vw: very weak site).

Although chemical metallocene–silanol interaction may be the main fixation mechanism of the catalyst on the zeolite, the presence of the physically adsorbed metallocene should not be discarded. Nanosized ZSM-2 zeolite has a large internal and external surface area (588 and 106 m^2 g^{-1}, respectively) as well as the largest zeolite pore aperture (0.74 nm), which favours the physical adsorption of the metallocene on the interior of the zeolite channels as well as on the outside surface of the zeolite crystal, as already found from HRTEM observations.

3.3. Ethylene polymerization on ZSM-2 zeolite-supported metallocene catalysts

Table 2 shows the results of ethylene polymerization activities obtained with the homogeneous and ZSM-2 zeolite-supported catalytic systems. For comparison, the metallocene catalyst was also fixed on commercial amorphous silica. As is generally known, the polymerization activity of supported catalysts is lower than that of the unsupported system. In this case the presence of diffusion-restricted metallocene species located on internal sites of the porous supports could be responsible for the lower activity of the heterogeneous catalysts. ZSM-2 (FAU/EMT) and FAU are the zeolite types with the largest pore aperture (0.74 nm) and with spacious internal cavities (1.3 nm in diameter); and although in principle metallocene activation and polymer growth from intracrystalline sites are feasible [23], these processes occur under a significant difusional control. It can also be seen that the activity

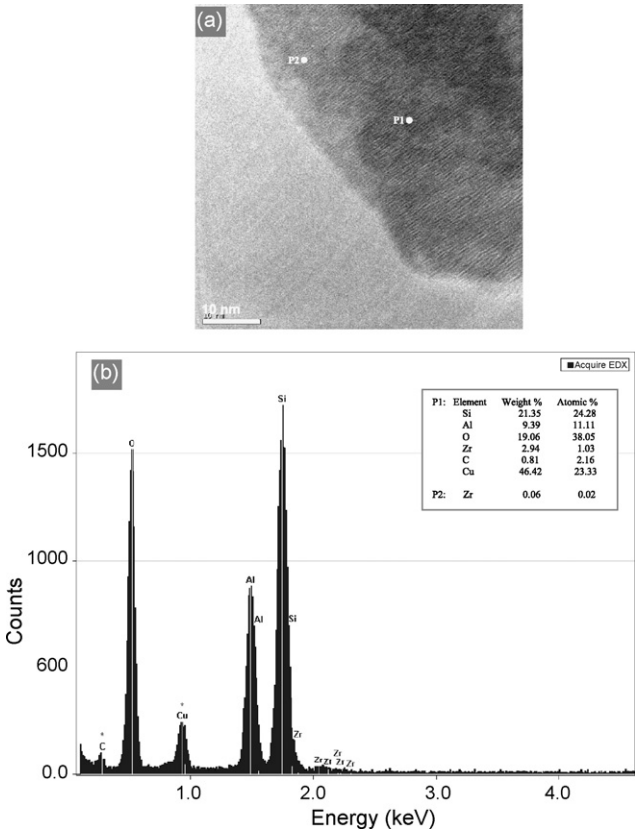

Fig. 4. HRTEM image of ZSM-2 zeolite-supported metallocene catalyst (a) and EDX elemental analysis on a selected point (b).

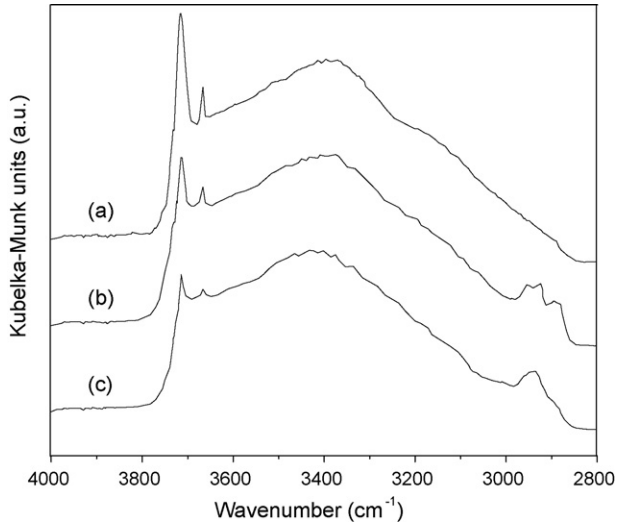

Fig. 5. DRIFT spectra of (a) ZSM-2 zeolite, (b) Cat/ZSM-2 and (c) Cat/MAO/ZSM-2 catalysts.

of the catalyst supported directly on ZSM-2 zeolite (Cat/ZSM-2) was higher than that of the catalyst supported on the MAO-treated zeolite (Cat/MAO/ZSM-2). Higher activity of Cat/zeolite catalyst with respect to that of Cat/MAO/zeolite catalyst has been also observed by other authors with catalysts supported on microsized Na-MOR and NaH-Y type zeolites [28], nevertheless relatively low activities were obtained by using these sodic zeolite forms (172–69 kg mol^{-1} Zr bar^{-1} h^{-1} at 50 °C). We agree with those authors in relation to that the presence of MAO on the zeolite surface has a deleterious effect on the polymerization activity because such a large molecule occupies zeolite sites where the metallocene could be directly and actively fixed. In addition, we also believe that the active metallocenium cation is better stabilized by the high density of negative charges of zeolite framework than by the MAO-modified zeolite surface. Fixation of the sizable MAO molecule on the zeolite surface has also a pore blocking effect, which is verified by the lower surface area and micropore volume of the MAO-treated ZSM-2 zeolite (S_g = 418 m^2 g^{-1}, V_o = 0.19 cm^3 g^{-1}) as compared with those of the untreated ZSM-2 zeolite (S_g = 558 m^2 g^{-1}, V_o = 0.26 cm^3 g^{-1}). As consequence of this zeolite pore blocking the amount of metallocene fixed on the MAO-treated ZSM-2 zeolite is also lower (0.18 wt.% Zr) than that fixed on the untreated ZSM-2 zeolite support (0.32 wt.% Zr). Thus, the results of the current work show that high polymerization activity can be obtained by directly supporting the metallocene on the nanosized ZSM-2 zeolite, and that no MAO treatment of this support is necessary prior to the fixation of the catalyst. In addition, the polymerization activity on ZSM-2 zeolite is increased when the metallocene is supported on the DEAL-ZSM-2 zeolite form (from 3579 to 4721 kg mol^{-1} Zr bar^{-1} h^{-1}). These results contrast with those obtained by using traditional silica as support, where it is found that MAO treatment of the silica is an essential step to obtain a supported catalyst with high activity. As is well known, the presence of MAO cocatalyst on the support surface aids in the fixation of the metallocene and contributes to its activation/stabilization, which is completed with the addition of soluble MAO into the reactor [15]. Because of that, the activation property of MAO is a consequence of its strong Lewis acidity. The types of acid sites existing on the ZSM-2 zeolite surface were investigated in order to clear the catalytic behaviour of this supported system. Fig. 6 shows the results of the DRIFT analysis of pyridine sorption on the supports that were studied. The DRIFT spectrum of pyridine sorbed on amorphous silica shows not peaks at 1455 or 1547 cm^{-1} attributed to Lewis or Brönsted acid sites, respectively. This result is expected considering the pure-silicon composition of the commercial support. The absence of strong acid sites on the silica surface was also confirmed by its low acid strength in potentiometric measurements (−140 mV). When silica was surface-treated with MAO, an intense DRIFT peak around 1460 cm^{-1} appears which is attributed to pyridine coordinated with Lewis acid sites existing on the sorbed MAO. This peak appears slightly shifted toward higher frequencies with respect to that found in most of the acid solids (∼1450 cm^{-1}), and this can be attributed to the effect of the complex chemical environment of the MAO structure [46]. In

Table 2
Ethylene polymerization results by using soluble metallocene and metallocene supported on ZSM-2 zeolite and commercial amorphous silica

Catalyst	Zr (%) (fixed)	Al (%) (support)	Activity (kg mol^{-1} Zr bar^{-1} h^{-1})	Productivity (g g^{-1} cat h^{-1})
Soluble catalyst	–	–	9647	–
Cat/MAO/ZSM-2	0.18	14.7	743	29
Cat/ZSM-2	0.31	11.4	3594	236
Cat/DEAL-ZSM-2	0.30	10.5	4721	375
Cat/SiO_2	0.19	–	959	40
Cat/MAO/SiO_2	0.93	3.34	4234	956

Reaction conditions: [Al(MAO)/Zr] = 1500, [Zr] = 6.7 × 10^{-6} mol/l, temperature = 60 °C, time = 0.5 h, solvent: 450 ml of toluene.

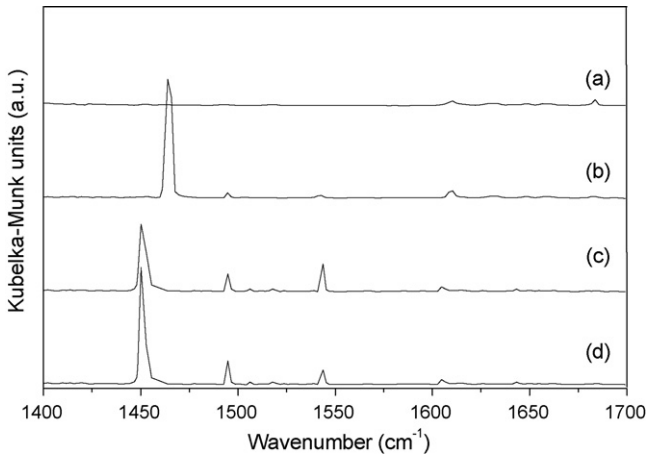

Fig. 6. DRIFT spectra of pyridine sorbed on (a) SiO_2, (b) MAO/SiO_2, (c) ZSM-2 and (d) DEAL-ZSM-2 catalyst supports.

the case of the ZSM-2 zeolite forms (Fig. 6c and d), the DRIFT spectra of pyridine sorption show the characteristic signals corresponding to both Lewis and Brönsted acid sites (1449 and 1545 cm^{-1}, respectively). The third band at 1490 cm^{-1} has been attributed to physisorbed pyridine [47], although it is also believed that this peak corresponds to a contribution of both Brönsted and Lewis acid sites [48]. It can be seen that ZSM-2 zeolite forms contain a predominant amount of Lewis acid-type acid sites on its surface; and that in the case of DEAL-ZSM-2 zeolite the amount of these Lewis acid sites seem to be similar to that found on MAO-treated silica (4 wt.%), as judged by the intensity of the 1449 and 1460 cm^{-1} bands. As is well known, the Lewis acidity of the zeolites is produced by the presence of extraframework aluminum species in their structure [26]. In the case of ZSM-2 zeolite, the formation of extraframework aluminum species is favoured by the calcination to which it is subjected during its preparation. When the zeolite is steam-dealuminated to obtain the DEAL-ZSM-2 zeolite form, the creation of strong Lewis acid sites increases, as has been discussed before. Thus, surface Lewis acidity of ZSM-2 zeolite comparable to that of MAO-treated silica can explain the high polymerization activity seen with the directly supported catalysts. Fig. 7 is a scheme of the most probable activation mechanism of the metallocene catalyst supported on DEAL-ZSM-2 zeolite. As already discussed, an important proportion of the metallocene catalyst is fixed on the hydroxyl groups of the zeolite surface, but in the case of DEAL-ZSM-2 zeolite, chloride from the $(n\text{BuCp})_2ZrCl_2$ metallocene may also interact with the cationic aluminum extraframe-

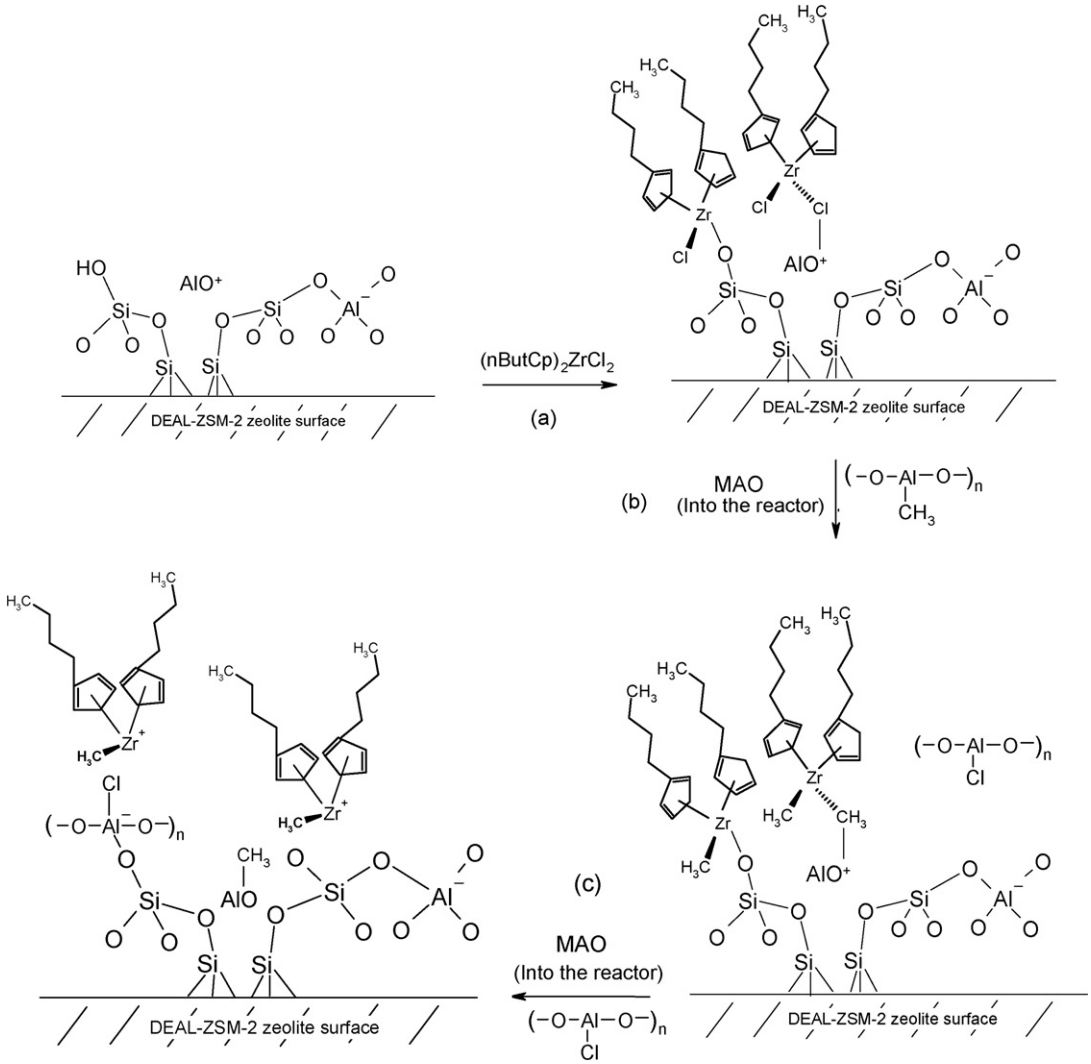

Fig. 7. Activation of metallocene catalyst on the DEAL-ZSM-2 zeolite surface: fixation of the metallocene on the zeolite surface (a), methylation of metallocene in the presence of MAO (b) and stabilization of the metallocenium cation by MAO and Lewis acid species of the zeolite (c).

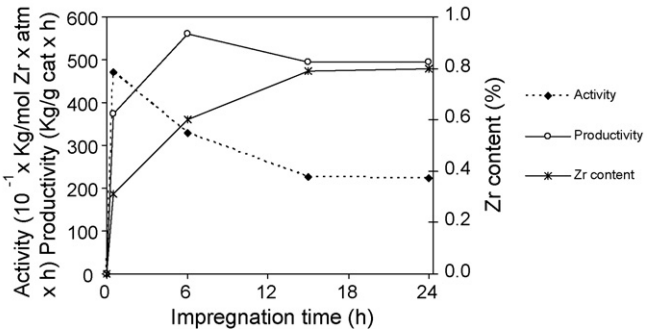

Fig. 8. Effect of impregnation time on the amount of fixed metallocene on DEAL-ZSM-2 zeolite and on the ethylene polymerization activity.

work species of the zeolite, thereby constituting an additional fixation pathway. When the supported catalyst is put in contact with MAO in the polymerization reactor, MAO causes methylation of the metallocene. Although different aluminum coordinations have been identified in the MAO structure [49], in this scheme the MAO structure is represented as $(–O–Al(CH_3)–O–)_n$ for greater clarity. Methylation of the metallocene is attributed to the methyl-donor tetracoordinated aluminum of the MAO structure, whereas the abstraction of chloride groups (and/or methyl) has been ascribed to tricoordinated aluminum. Stabilization of the metallocenium cation formed is carried out through ion-pair formation with a negatively charged specie of MAO sorbed on the zeolite surface, as proposed by Hlatky [12] for the activation of metallocenes supported on silica. In addition to this MAO activating/stabilizing effect, the presence of aluminum species with strong Lewis acidity on the DEAL-ZSM-2 zeolite surface (AlO^+) should also significantly contribute to the activation of the metallocene. Lewis acid sites of zeolite can participate in the abstraction of the labile groups of the metallocene (methyl and/or chloride), favouring the formation of the metallocene active species. The active metallocenium cation is also further stabilized through the negatively charged zeolite framework.

A comment about the polymerization productivity values shown in Table 2 will also be made here. Obviously, catalysts with higher zirconium content have higher production of polyethylene per mass of supported catalyst. It can also be seen that although ZSM-2- and DEAL-ZSM-2-supported catalysts have similar zirconium content, Cat/DEAL-ZSM-2 shows a higher productivity value. In addition to the already discussed surface–Lewis acid effect, DEAL-ZSM-2 zeolite has a higher degree of mesoporosity in its structure (Table 1), which can improve accessibility to the internal active sites during the reaction.

The effect of impregnation time on the amount of fixed metallocene on DEAL-ZSM-2 zeolite and on polymerization activity was also evaluated. Fig. 8 shows that higher impregnation time during the preparation of Cat/DEAL-ZSM-2 increases the fixation of zircocene on the zeolite. A maximum zirconium content of around 0.8 wt.% is reached after 15 h of impregnation, which indicates that kinetic-difussion phenomena may control the fixation of the metallocene within the zeolite pores. Although the zirconium content of the DEAL-ZSM-2 zeolite-supported catalyst can be increased, that does not cause an increase in the polymerization activity; rather these catalysts exhibit lower activity than that of the initial catalyst (0.5 h, 0.31 wt.% Zr). These results can be understood considering the diffusion phenomena than intervene during the polymerization reaction on supported catalysts. Higher impregnation times should increase the amount of metallocene fixed on the internal surface of the zeolite; thus the activation of internally fixed metallocene may be restricted by the diffusional limitations imposed by zeolite pore apertures on the sizable MAO cocatalyst. Moreover, the growth of the polyethylene chain from active sites located on the internal pore surface can be also affected, thus decreasing the activity. Diffusion effects during polymerization reactions on zeolite-supported metallocene catalysts have also been detected by other authors using traditional microsized zeolites [28,29,50], for which relatively low activity values have been reported (122–1118 kg mol^{-1} Zr bar^{-1} h^{-1}). In the present study, we think that the high external surface area of nanosized ZSM-2 zeolite makes it possible to increase the amount of metallocene fixed on the external zeolite surface, and thus produces a less diffusion-controlled polymerization from external active sites.

On the other hand, as expected, productivity values increased with zirconium content up to a maximum value of 559 g g^{-1} cat h^{-1} for a zirconium content of 0.6 wt.%. Higher zirconium loadings tended to decrease productivity, an effect that can be attributed to the well-known bimolecular deactivation reactions between neighbour zircocenes [51,52], which in this case are favoured by the increased metallocene concentration on the zeolite surface.

Table 4
Characterization of polyethylene obtained on ZSM-2 zeolite-supported catalysts

Catalyst	Cocatalyst	M_w (kg mol^{-1})	M_w/M_n	T_m (°C)	X_C (%)
Homogeneous	MAO	336	1.77	137	72
Cat/MAO/ZSM-2	MAO	342	1.76	138	67
Cat/DEAL-ZSM-2	MAO	287	1.96	139	77
Cat/DEAL-ZSM-2	TMA	245	1.95	139	79

3.4. Ethylene polymerization on the Cat/DEAL-ZSM-2 catalyst using TMA as cocatalyst

In order to evaluate the activity of Cat/DEAL-ZSM-2 catalyst in the presence of an activator less expensive than MAO, polymerization reactions were carried out by using trimethylaluminum (TMA) as cocatalyst. The results obtained with different Al(TMA)/Zr ratios are shown in Table 3, compared to those reported for other active supported systems in the presence of an alkylaluminum. It can be seen that activity values in the presence of TMA are lower

Table 3
Comparison of ethylene polymerization activity of Cat/DEAL-ZSM-2 catalyst with reported active systems in the presence of trialkyaluminums

Catalyst support	Metallocene	AlR_3	AlR_3/Zr	Activity (kg mol^{-1} Zr bar^{-1} h^{-1})
DEAL-ZSM-2 zeolite	$(n\text{BuCp})_2ZrCl_2$	TMA	1500	518
DEAL-ZSM-2 zeolite	$(n\text{BuCp})_2ZrCl_2$	TMA	2780	2073
DEAL-ZSM-2 zeolite	$(n\text{BuCp})_2ZrCl_2$	TMA	3023	1555
TMA-treated clay [48]	Cp_2ZrCl_2	TMA	2000	1350[a]
$B(C_6F_5)_3$-functionalized silica [16]	Cp_2ZrCl_2	TIBA	595[b]	2930[a]
FSO_3H-functionalized SBA-15 silica [17]	$((CH_3)_5Cp)_2Zr(CH_3)_2$	TMA	700	202[a]

[a] Reported activity values were normalized with the ethylene pressure value used in the reaction.
[b] A no-informed amount of TIBA was also added into the reactor to scavenge impurities.

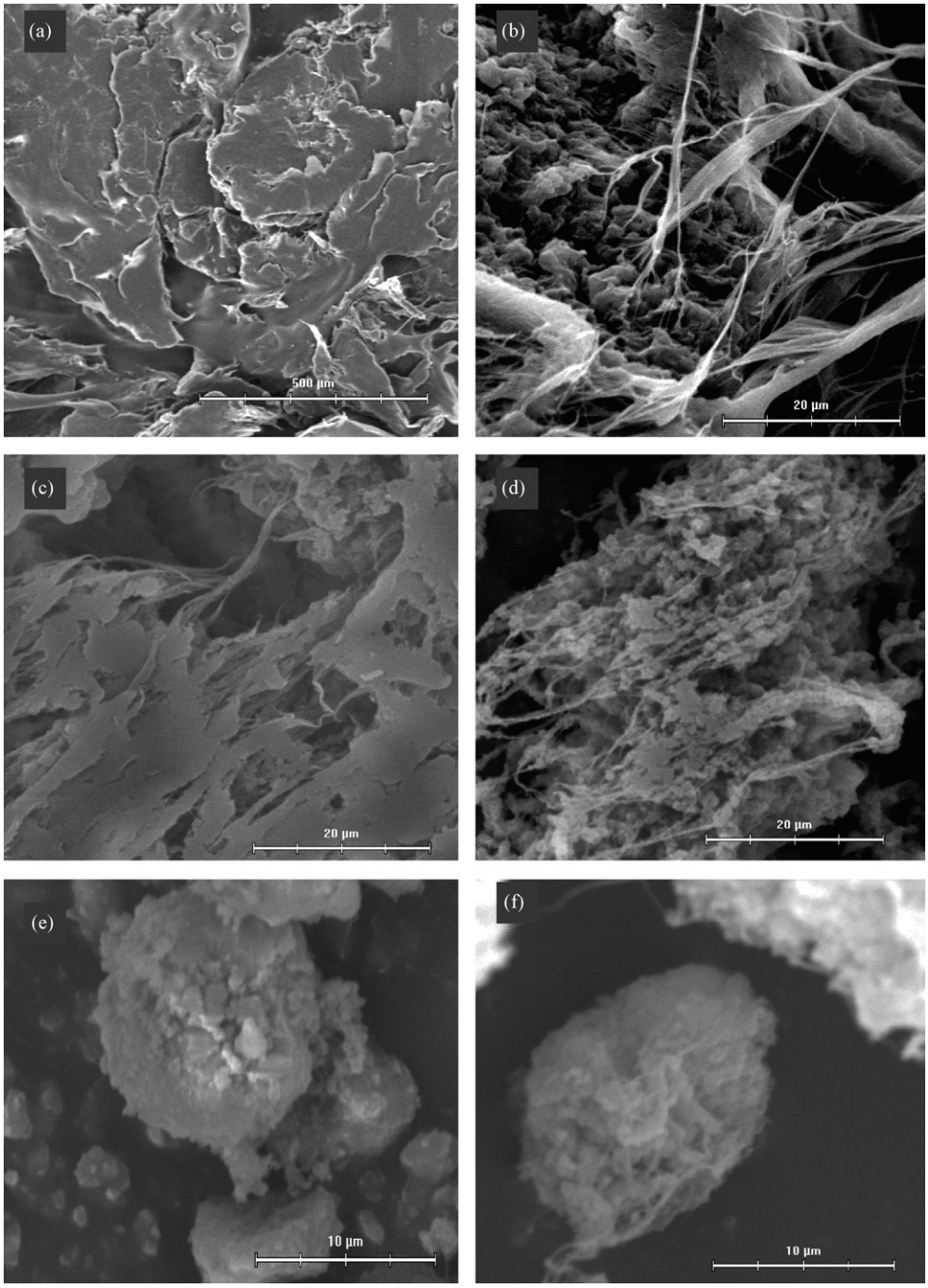

Fig. 9. SEM images of polyethylene obtained on homogeneous catalyst (a and b), and on DEAL-ZSM-2 supported catalyst by using MAO (c and d) and TMA (e and f) as cocatalyst in the reactor.

than those obtained with MAO as cocatalyst (Table 3). This difference is expected, since alkylaluminums are known to be weaker activators than MAO [53,54]. The highest activity value (2073 kg mol^{-1} Zr bar^{-1} h^{-1}) was obtained using an Al(TMA)/Zr ratio of 2780; beyond this value it was found that polymerization activity tends to decrease; perhaps due to the "poisoning" effect observed for TMA [55]. In order to make a more appropriate comparison with the reported information, all activity values were normalized with respect to the ethylene pressure used. It is seen that the activity of the Cat/DEAL-ZSM-2 system in the presence of TMA is higher than that of some reported systems, and close to that of $B(C_6F_5)_3$-functionalized silica. In this comparison, differences in the type of metallocene, AlR_3/Zr ratio values, and in the procedures used for mixing the reaction components should also be taken into account. Regarding the role of the alkylaluminum in these free-MAO active systems; in the case of the TMA-treated clay [56], the authors comment that TMA reacts with OH groups of clay derived-acid silica layers and with the metallocene to form an active catalyst. In the $B(C_6F_5)_3$-functionalized silica system [24], it is suggested that triisobutylaluminum (TIBA) has the dual role of scavenging the impurities as well being the alkylating agent for dichlorinated metallocene. In the case of FSO_3H-functionalized SBA-15 silica [25], the authors propose an activation mechanism in which TMA reacts with the SBA-FSO_3H Brönsted acid surface and

creates a surface-tethered species that can activate the metallocene. In the present study, we think that TMA plays a role similar to that described for MAO in the Cat/DEAL-ZSM-2/MAO system (Fig. 7). Thus, TMA is responsible of the alkylation of the dichlorinated metallocene, and in conjunction with the extra-framework aluminum species of the zeolite it leads to the stabilization of the active metallocenium cation.

3.5. Characterization of polyethylene products

Polyethylene (PE) products were characterized by GPC and DSC. Molecular weight (M_w), polydispersity (M_w/M_n), and melting temperature (T_m) of the polymers are presented in Table 4. It is seen that PE obtained with the catalyst supported on MAO-treated zeolite (Cat/MAO/ZSM-2) does not show significant differences compared to that from the homogeneous system. As mentioned above, MAO sorbed on the zeolite surface may block the fixation of the metallocene in the interior of the zeolite pores. Thus, externally fixed metallocene can be more easily leached from the support when placed in contact with the soluble MAO in the reactor [57]. This leaching phenomenon could be responsible for the production of PE with "homogeneous" characteristics. PE products obtained with catalysts directly supported on DEAL-ZSM-2 tend to have lower molecular weight and higher polydispersity values. Molecular weight of metallocene-synthesized polyolefins is dependent on the type of active site and on the differences in the geometries assumed by the transition states of the propagation reaction and of the β-transfer to monomer [3]. The different nature of the active sites existing on the ZSM-2 zeolite surface could to favour the transfer/termination reactions decreasing thus the molecular weight of the polymer as compared with that obtained from active sites formed with the soluble metallocene. Although, immobilization of metallocene may also to determine the production of higher molecular weight polymer as consequence of a reduction of the bimolecular deactivation reactions between neighboring zircocene sites; polymer growth from active sites located within the zeolite cavities may to increase the probability of chain transfer or termination reactions, resulting in lower molecular weight polymers. Lower molecular weights were particularly obtained when TMA was used as cocatalyst. This result is a consequence of the proved ability of TMA to act as a chain-transfer agent [53]. On the other hand, no significant differences were found in the melting temperature of the different polyethylenes. The slightly higher crystallinity of PE obtained on DEAL-ZSM-2-supported catalysts may be due to the effect of the zeolite crystal structure during polymer growth from internal sites of the zeolite crystal.

Polyethylene products were also examined by SEM microscopy (Fig. 9). PE obtained with homogeneous catalysts had a fibrous morphology (Fig. 9a and b). When the DEAL-ZSM-2-supported catalyst was used with MAO as cocatalyst, a mixture of fibrous PE with more particulate or powdered PE was obtained (Fig. 9c and d). The SEM image of the powdered fraction (Fig. 9d) shows the presence of particles of the zeolite support in the polymer matrix. This indicates that the powdered PE fraction is produced by preferential growth of the polymer from the zeolite-supported catalyst, whereas the fibrous PE fraction can be attributed to "homogeneous" PE grown from MAO-leached catalyst. In the case of PE obtained from the Cat/DEAL-ZSM-2 catalyst in the presence of TMA, only a powdered PE product was obtained (Fig. 9e and f). The SEM micrographs of these products show that polymer grown around zeolite particles takes on a sphere-like morphology. Because ZSM-2 zeolite nanoparticles have a hexagonal plate-like morphology; the observed spherical morphology of PE particles may be induced by a core of agglomerated ZSM-2 zeolite nanoparticles. The PE particles are around 10 μm in size, or about 6 times smaller than that of polypropylene obtained on silica-supported catalysts (~60 μm) [15], showing an effect caused by the nanosized zeolite support. Regarding the greater influence of the zeolite support on PE morphology when TMA is used, the smaller size of TMA molecules would allow the metallocene fixed inside the zeolite cavities to be more efficiently activated than when MAO is used. Therefore, the TMA-activated system favours polymer chain growth from within the zeolite crystals, thereby increasing the influence of the zeolite support on the final PE morphology.

4. Conclusions

Nanosized ZSM-2 zeolite can be prepared with adequate Lewis acid properties for use as an active support of ethylene polymerization catalysts. Metallocene catalysts directly supported on dealuminated (DEAL) ZSM-2 zeolite exhibits high activity values. Metallocene activation is attributed to the action of soluble MAO in the reactor and to the activator effect of extraframework aluminum species with strong Lewis acidity existing in the DEAL-ZSM-2 zeolite structure. The large external surface area of the nanosized zeolite support also contributes to reduce the unfavourable diffusion effects commonly observed in microsized zeolites.

The DEAL-ZSM-2-supported catalyst also had polymerization activity using a trialkylaluminum (TMA) instead of MAO as cocatalyst. Furthermore, the use of a smaller TMA activator molecule appears to favour the effect of the zeolite support on the morphology of the resulting polymer particles.

The results of this work show that the DEAL-ZSM-2 zeolite support does not need to be treated with MAO before fixation of the metallocene catalyst, and that polymerization activity can also be achieved using a trialkyaluminum as cocatalyst. Thus, the use of DEAL-ZSM-2 zeolite as metallocene support may contribute to reduce the amount of MAO required for ethylene polymerization.

Acknowledgements

The authors acknowledge the financial support of CONICYT through FONDAP Project No. 11980002 and through FONDECYT Project No. 11060384 (R. Rojas). We also thank Dr. Jose Luis Arias' Laboratory (Departamento de Ciencias Veterinarias y Pecuarias, Universidad de Chile) for SEM facilities.

References

[1] K. Weiss, S. Botzenhardt, M. Hofmann, in: W. Kaminsky (Ed.), Metalorganic Catalysts for Synthesis and Polymerization: Recent Results by Ziegler-Natta and Metallocene Investigations, Springer Verlag, Heidelberg, 1999, pp. 97–100.
[2] H.H. Brintzinger, D. Fischer, R. Mulhaupt, B. Rieger, R.M. Waymouth, Angew. Chem. Int. Ed. Engl. 34 (1995) 1143–1170.
[3] L. Resconi, L. Cavallo, A. Fait, F. Piemontesi, Chem. Rev. 100 (2000) 1253–1345.
[4] R. Quijada, J. Dupont, D.C. Silveira, M.M. Lacerda, R. Scipioni, Macromol. Rapid Commun. 16 (1995) 357–362.
[5] R. Quijada, R. Rojas, R.S. Mauler, G.B. Galland, R.B. Scipioni, J. Appl. Polym. Sci. 64 (1997) 2567–2574.
[6] R. Benavente, E. Perez, R. Quijada, J. Polym. Sci.: Polym. Phys. 39 (2001) 277–285.
[7] R. Quijada, J.L. Guevara, M. Yazdani-Pedram, G.B. Galland, D. Ribeiro, Polym. Bull. 49 (2002) 273–280.
[8] R. Quijada, R. Rojas, L. Alzamora, J. Retuert, F.M. Rabagliati, Catal. Lett. 46 (1997) 107–112.
[9] R. Quijada, R. Rojas, A. Nárvaez, L. Alzamora, J. Retuert, F.M. Rabagliati, Appl. Catal. A 166 (1998) 207–214.
[10] D. Bianchini, G.B. Galland, J.H. Dos Santos, R.J.J. Williams, D.P. Fasce, I.E. dell'Erba, R. Quijada, M. Pérez, J. Polym. Sci. Part A: Polym. Chem. 43 (2005) 5465–5476.
[11] E. Moncada, R. Quijada, J. Retuert, J. Appl. Polym. Sci. 103 (2007) 698–706.
[12] G.G. Hlatky, Chem. Rev. 100 (2000) 1347–1376.
[13] E. Zurek, T. Ziegler, Prog. Polym. Sci. 29 (2004) 107–148.
[14] J.H.Z. dos Santos, C. Krug, M. Barbosa da Rosa, F. Chiarello, J. Dupont, M. de Camargo, J. Mol. Catal. A: Chem. 139 (1999) 199–207.

[15] G. Fink, B. Steinmetz, J. Zechlin, C. Przybyla, B. Tesche, Chem. Rev. 100 (2000) 1377–1390.
[16] D. Liua, S. Wanga, H. Wanga, W. Chena, J. Mol. Catal. A: Chem. 246 (2006) 53–58.
[17] I. Tritto, L. Boggioni, M.C. Sacchi, T. Dall'Occo, J. Mol. Catal. A: Chem. 204–205 (2003) 305–314.
[18] A. Yano, S. Hasegawa, S. Yamada, A. Akimoto, J. Mol. Catal. A: Chem. 148 (1999) 77–86.
[19] F. Focante, P. Mercandelli, A. Sironi, L. Resconi, Coord. Chem. Rev. 250 (2006) 170–188.
[20] N.F. Brockmeler, in: G.M. Benedikt, B.L. Goodall (Eds.), Metallocene-catalyzed Polymers: Materials, Properties, Processing & Markets, Plastics Design Library, New York, 1998, pp. 11–12.
[21] H. Ahn, T.J. Marks, J. Am. Chem. Soc. 120 (1998) 13533–13534.
[22] C.P. Nicholas, H. Ahn, T.J. Marks, J. Am. Chem. Soc. 125 (2003) 4325–4331.
[23] H. Nakano, T. Takahashi, H. Huchino, T. Tayano, T. Sugano, in: T. Shiono, K. Nomura, M. Terano (Eds.), Progress in Olefin Polymerization Catalysts and Polyolefin Materials, Studies in Surface Science & Catalysis, vol. 161, Elsevier, Amsterdam, 2006, pp. 19–22.
[24] S. Charoenchaidet, S. Chavadej, E. Gulari, J. Mol. Catal. A: Chem. 185 (2002) 167–177.
[25] J.C. Hicks, B.A. Mullis, C.W. Jones, J. Am. Chem. Soc. 129 (2007) 8426–8427.
[26] J. Weitcamp, M. Hunger, in: J. Čejka, H. van Bekkum, A. Corma, F. Schüth (Eds.), Introduction to Zeolite Science and Practice, Studies in Surface Science & Catalysis, vol. 168, Elsevier, Amsterdam, 2007, pp. 787–804.
[27] M. Michelotti, A. Altomare, F. Ciardelli, E. Roland, J. Mol. Catal. A: Chem. 129 (1998) 241–248.
[28] Y.S. Ko, S.I. Woo, Eur. Polym. J. 39 (2003) 1553–1557.
[29] S.C. Moreira, M.F.V. Marques, Eur. Polym. J. 37 (2001) 2123–2130.
[30] S.C. Moreira, M.F.V. Marques, J. Mol. Catal. A: Chem. 192 (2003) 93–101.
[31] V.I. Costa Vayá, P.G. Belelli, J.H.Z. dos Santos, M.L. Ferreira, D.E. Damiani, J. Catal. 204 (2001) 1–10.
[32] L. Tosheva, V.P. Valtchev, Chem. Mater. 17 (2005) 2494–2513.
[33] J. Ciric, U.S. Patent 3,411,874 (1968).
[34] R.M. Barrer, W. Sieber, J. Chem. Soc., Dalton Trans. (1977) 1020–1026.
[35] B.J. Schoeman, J. Sterte, J. Otterstedt, J. Colloid Interface Sci. 170 (1995) 449–456.
[36] J.A. Martens, Y.L. Song, E.J.P. Feijen, P.J. Grobet, P.A. Jacobs, J. Phys. Chem. 97 (1993) 5132.
[37] Ch. Baerlocher, L.B. McCusker, D.H. Olson, Atlas of Zeolite Framework Types, sixth revised ed., Elsevier, Amsterdam, 2001.
[38] C. Covarrubias, R. García, R. Arriagada, J. Yánez, H. Ramanan, Z. Lai, M. Tsapatsis, J. Membr. Sci. 312 (2008) 163–173.
[39] R. Cid, G. Pecchi, Appl. Catal. 14 (1985) 15–21.
[40] G.T. Kerr, A.W. Chester, D.W. Olson, Proc. Symp. Zeolites, Szeged (1978) 169.
[41] U. Lohse, M. Mildebrath, Z. Anorg. Allg. Chem. 476 (1981) 126–135.
[42] G.T. Kerr, in: W.M. Meier, J.B. Uytterhoeven (Eds.), Molecular Sieves, Advances in Chemistry, Series 121, American Chemical Society, Washington, 1973, p. 219.
[43] P.A. Jacobs, H.K. Beyer, J. Phys. Chem. 83 (1979) 1174–1177.
[44] S.P. Zhdanov, T.I. Titova, L.S. Kosheleva, W. Lute, Pure Appl. Chem. 61 (1989) 1977–1980.
[45] G. González, C.S. González, W. Stracke, R. Reichelt, L. García, Microporous Mesoporous Mater. 101 (2007) 30–42.
[46] E.Y. Chen, T.J. Marks, Chem. Rev. 100 (2000) 1391–1434.
[47] Z.S. Seddigi, React. Kinet. Catal. Lett. 73 (2001) 63–70.
[48] A. Rahman, G. Lemay, A. Adnot, S. Kaliaguine, J. Catal. 112 (1988) 453–463.
[49] M.L. Ferreira, P.G. Belelli, A. Juan, D.E. Damiani, Macromol. Chem. Phys. 201 (2000) 1334–1344.
[50] Y.S. Ko, T.S. Seo, D.S. Hong, S.I. Woo, in: W. Kaminsky (Ed.), Metalorganic Catalysts for Synthesis and Polymerization: Recent Results by Ziegler-Natta and Metallocene Investigations, Springer Verlag, Heidelberg, 1999, pp. 368–380.
[51] D.H. Lee, H.B. Lee, S.K. Noh, B.K. Song, S.M. Hong, J. Appl. Polym. Sci. 71 (1999) 1071–1080.
[52] J.H.Z. Dos Santos, P.P. Greco, F.C. Stedile, J. Dupont, J. Mol. Catal. A: Chem. 154 (2000) 103–113.
[53] L. Resconi, S. Bossi, L. Abis, Macromolecules 23 (1990) 4489–4491.
[54] I. Tritto, S. Li, M.C. Sacchi, G. Zannoni, Macromolecules 26 (1999) 7111–7115.
[55] J. Pédeutour, K. Radhakrishnan, H. Cramail, A. Deffieux, J. Mol. Catal. A: Chem. 185 (2002) 119–125.
[56] K. Weiss, C. Wirth-Pfeifer, M. Hofmanna, S. Botzenhardt, H. Langb, K. Brüning, E. Meichel, J. Mol. Catal. A: Chem. 182–183 (2002) 143–149.
[57] M.W. McKittrick, K. Yu, C.W. Jones, J. Mol. Catal. A: Chem. 237 (2005) 26–35.